IEEE Access
Multidisciplinary ⋮ Rapid Review ⋮ Open Access Journal

Received 14 December 2023, accepted 30 December 2023, date of publication 8 January 2024,
date of current version 12 January 2024.

Digital Object Identifier 10.1109/ACCESS.2024.3350729

RESEARCH ARTICLE

Cophase Traction Power Supply System Based on Improved MMC-STATCOM-Vv Wiring

YONG ZHOU[1], MINAN TANG[1], (Senior Member, IEEE), AND WEILI LIU[2]
[1]College of Automation and Electrical Engineering, Lanzhou Jiaotong University, Lanzhou 730070, China
[2]Zhejiang Zhonghe Technology Corporation, Hangzhou 310000, China

Corresponding author: Yong Zhou (11200393@stu.lzjtu.edu.cn)

This work was supported in part by the National Natural Science Foundation of China under Grant 61663021, Grant 71763025, and Grant 61861025; and in part by the Project of Gansu Basic Research Innovation Group, China, under Grant 18JR3RA133.

ABSTRACT A static synchronous compensator topology with an improved MMC (MMC-STATCOM) is proposed in this study after analyzing the modular converter (MMC) topology. The improved MMC uses fewer low-voltage power switching elements and is more economical compared to the traditional MMC. In the traction power supply environment without balancing equipment, the DC-side voltage balancing control of the converter is studied in depth, and a three-level control strategy is established. The first level of control is total voltage control, which achieves energy exchange between the converter and the power system through active power to achieve DC-side voltage balance. The second level of control is phase-to-phase voltage balancing control, which achieves phase-to-phase power redistribution by injecting zero-sequence voltage into the new topology converter. The third level of control is the intra-phase voltage balancing control, which ensures that the intra-phase module DC-side voltage is equal to the given value by controlling the DC voltage of each phase sub-module. In the same phase power supply environment, the compensation capability of the improved converter is analyzed to derive the compensation relationships for each port, and the compensation targets are achieved. Finally, the correctness of the control strategy and the compensation capability of the improved converter structure are verified by simulation experiments.

INDEX TERMS DC-side voltage control, modular multilevel converter, static synchronous compensator, traction power supply.

I. INTRODUCTION

Since its introduction by German scholars R. Marquardt and A. Lesnicar, the modular multilevel converter (MMC) has been commonly studied and applied in the comprehensive management of power quality in power supply systems [1], [2], [3], [4]. The MMC has become an outstanding topology for medium-voltage, high-power energy conversion applications due to its remarkable modular structure, good scalability, excellent harmonic management performance, and performance for high-power applications through cascaded topologies as well as the potential for the development of cascaded topologies for high-power applications. Despite the many advantages of the MMC topology, its control is challenging [5], [6].

The MMC is composed of a cascade of several sub-modules to achieve the use of low-voltage switching elements in high-voltage environments. The number of sub-modules can be changed to match different voltage levels according to the actual environmental requirements, which is a unique advantage not only in managing the power quality of the grid but also in managing the power quality of the traction power supply [7], [8], [9], [10]. However, in terms of economic cost, the MMC topology uses a large number of low-voltage power switching components, resulting in high cost and low economy. At present, owing to the outstanding advantages of MMC topology, many scholars have studied the application of MMC topology in the design of the static synchronous compensator (STATCOM), and the research has mainly focused on DC-side voltage balance control, compensation control, and the loop current problem existing in the bridge arm [11], [12], [13], [14], [15], [16], [17], [18], [19].

The associate editor coordinating the review of this manuscript and approving it for publication was Diego Bellan.

Reference [20] deeply analyzed the energy relationship between phases, upper bridge arm and lower bridge arm, and sub-module of MMC structure, investigated the causes of DC-side voltage unbalance, and added a circulation suppression part based on the original DC-side control method to achieve the DC-side voltage balance. Reference [21] investigated the principle of loop formation between the upper and lower bridge arms of the MMC topology and proposed a general loop suppression strategy for the MMC topology. Reference [22] discussed the operation of a STATCOM based on a cascaded H-bridge (CHB) converter under unbalanced grid conditions, where a zero-sequence voltage term is injected into the converter to keep the capacitive voltages of the sub-modules balanced. Reference [23] presented a synchronizer-based STATCOM with self-synchronization and voltage imbalance compensation.

This paper proposes an improved MMC topology that combines MMC and STATCOM, which adds a set of H-bridges to the half-bridge arm module of the traditional MMC structure, and it reduces the number of bridge arm IGBTs used in the improved MMC structure with better economy. For the DC-side voltage balancing control of the improved MMC converter, this paper establishes a three-level control system for DC-side voltage in the grid environment to ensure that the improved MMC-STATCOM converter can work stably to compensate for the three-phase balancing of the power system. In the same phase power supply environment, the improved MMC-STATCOM converter ensures the power supply quality of locomotives. Finally, the feasibility of this structure and the effectiveness of the DC-side voltage control method in two power supply environments are verified by simulation.

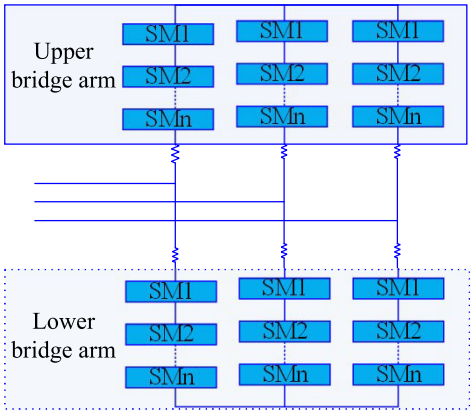

FIGURE 1. Basic structure of MMC.

II. IMPROVE THE TOPOLOGY OF MMC-STATCOM

Fig.1 shows the basic three-phase MMC topology, where in each phase is divided into upper and lower bridge arms, each of which is cascaded by N sub-modules composed of two IGBTs. Theoretically, when more sub-modules are cascaded in the three-phase bridge arm, the output voltage of the three-phase bridge arm becomes more sinusoidal, and the harmonic content is lower. After analyzing the basic structure circuit of MMC in this paper, the three-phase MMC structure is improved, and the improved structure is shown in Fig.2. The improved MMC-STATCOM structure uses only the three-phase MMC half-bridge arm structure, and an H bridge is added to the half-bridge arm for DC to AC conversion. This structure can greatly reduce the number of switching power devices under the same output condition compared with the three-phase MMC structure; furthermore, there is no loop current problem between the bridge arms, so the loop current problem does not need to be considered in the control strategy of MMC. In addition, cascaded converters are generally used in medium and high voltage environments, so the modified MMC-STATCOM structure and H-bridge structure with gate turn-off thyristor (GTO) are chosen.

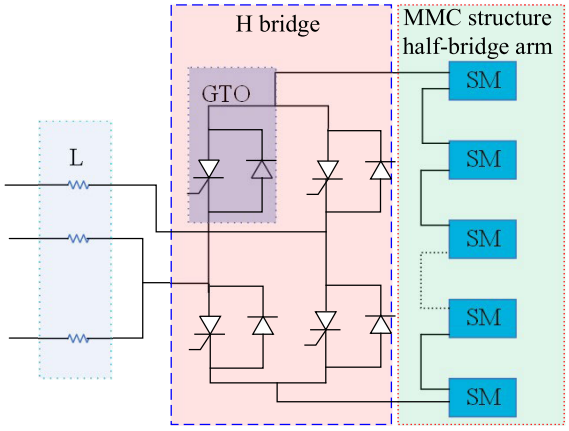

FIGURE 2. Topological structure block diagram of the improved MMC-STATCOM.

Topology analysis is conducted to compare the number of devices used in multilevel converters. The more common cascaded H-bridge and the topologies shown in Figs.1 and 2 are selected for comparison. The comparison results are shown in Table 1.

TABLE 1. Comparison of the number of components used in each topology.

Name	Cascaded H-bridge	Traditional half bridge MMC	Improve MMC structure
Level	2K+1	2K+1	2K+1
Capacitance	0	0	0
Diode	K	2K	K
Switches	4K	4K	2K+4

As can be seen from Table 1, the proposed scheme in this paper can reduce the number of power switching devices in the case of generating the same number of levels, which lowers the cost of the converter.

III. IMPROVED MODULATION AND CONTROL STRATEGY OF MMC-STATCOM

A. CARRIER PHASE SHIFT MODULATION

Carrier phase shifted sinusoidal pulse width modulation (CPS-SPWM) is a pulse width modulation method that uses a

carrier signal with a certain phase relationship for pulse width modulation to reduce the total harmonics injected into the system by multiple commutated bridges with a series-parallel relationship [24], [25], [26], [27].

Specifically, in the improved MMC topology with N cascaded sub-modules, the frequency and amplitude of the corresponding delta wave of each sub-module are unchanged, the delta carrier wave phase difference is π/N, and the improved MMC topology only uses the half-bridge arm of the basic three-phase MMC structure. Hence, the modulating wave takes an absolute value, each unit sub-module also uses the same modulating wave, the number of voltage levels output from the improved cascaded sub-module is $N + 1$, the output waveform is a steamed bun wave, and the number of output levels becomes $2N + 1$ by the H-bridge. U_0 is the H-bridge output voltage, with N being 3, for example, the number of levels output from the H-bridge is 7, and the waveform of the number of levels is shown in Fig.3.

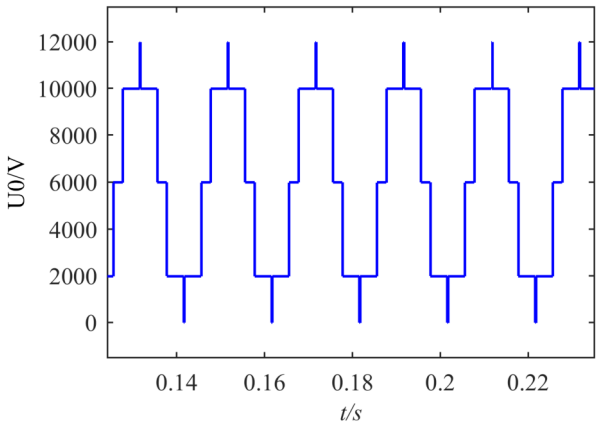

FIGURE 3. Carrier phase shift modulation waveform.

B. IMPROVED CONTROL STRATEGY OF MMC-STATCOM

In a traction power supply environment without balancing equipment, where three-phase power asymmetry or electric locomotives can make negative sequence components appear in the power system, the MMC-STATCOM's DC-side voltage must be controlled to ensure that the improved MMC-STATCOM can work stably.

Fig.4 shows the overall control block diagram of the modified MMC-STATCOM. The control system consists of capacitor voltage control and current tracking control on the DC side. The voltage control mainly keeps the DC side voltage stable. The control system is established using the reactive power detection method based on the instantaneous power theory. It is used to detect the load current and the total voltage control, which are then used to obtain the reactive current command value and the active current command value, respectively, and then the current reference value is decoupled by the dq state to realize the dynamic tracking of the current.

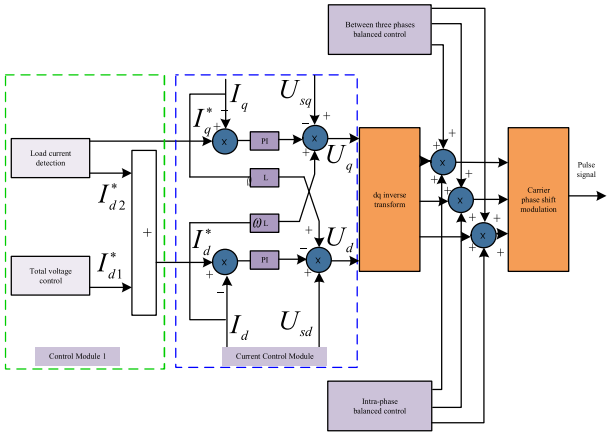

FIGURE 4. Overall block diagram of the control system.

Overall, a DC control method is used for the modified MMC-STATCOM converter, where the DC-side voltage is the outer loop and the current is the inner loop. To make the capacitor voltage on the DC side balanced and stable, three levels of control are used in this paper. The first level of control is total voltage control; the second level of control is phase-to-phase voltage balancing control; and the third level of control is intra-phase voltage balancing control.

C. DC SIDE TOTAL VOLTAGE CONTROL

Fig.5 shows the block diagram of the DC-side total voltage control. Theoretically, the converter is lossless,This control method exchanges active power with the grid through the modified MMC-STATCOM converter to ensure that the overall active power of the converter is constant and the DC voltage is constant.

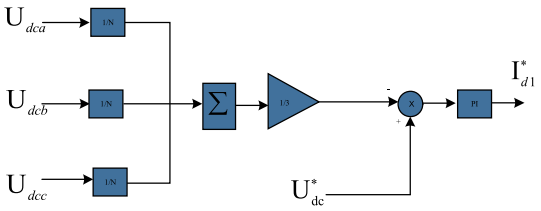

FIGURE 5. Topological structure block diagram of the improved MMC-STATCOM.

Analyzing the block diagram of DC-side total voltage control, this control method first detects the single-phase half-bridge structure module capacitor voltage values U_{dc} of A, B and C phases of the improved MMC-STATCOM, calculates the average value U_{ave}, uses the proportional-integral (PI) controller to adjust and process the difference between the average value U_{ave} and and the reference command value U^*_{dc} to obtain the active current command value I^*_{d1} of the fundamental wave and uses the active current command value I^*_{d1} as the energy exchange command of the improved MMC-STATCOM. The active current command value I^*_{d1} is then decoupled by the PI controller to achieve the tracking

of the active current command value I_{d1}^*, and finally, the average value of the total voltage is balanced with the given value. After the load current detection, the reactive current value command value I_{d2}^* is obtained based on the instantaneous reactive power theory. Then the active current command value I_{d1}^* and the reactive current command value I_{d2}^* are summed to obtain the final command current value. In the total voltage balance control, when U_{ave} is less than U_{dc}^*, the improved MMC-STATCOM converter absorbs the corresponding active power from the grid so that the average value of the module capacitor voltage U_{ave} and the reference command value U_{dc}^* can be balanced. On the contrary, when U_{ave} is greater than U_{dc}^*, the main circuit of the converter releases the corresponding active power to the grid, so that the average value of the module capacitor voltage U_{ave} drops to the reference command value U_{dc}^* to reach the dynamic balance.

D. PHASE-TO-PHASE BALANCE CONTROL

Improving the different losses of each switching element in the MMC-STATCOM converter and the different charging and discharging times of the submodules make the DC-side voltage unstable. The first level of control is the DC-side total voltage control, which makes the capacitor voltage on the DC side of the converter stable near the reference command value and the capacitor voltage on the DC side stable near the reference value U_{dc}^*. When the three-phase imbalance is serious, the DC voltages of each phase of the converter have large differences. If these voltages are not controlled, the sub-modules perform poorly, and the switching devices may be damaged due to overvoltage. Specifically, a high DC-side voltage causes each phase module to overwork and the switching devices to burn out due to overvoltage, and a low DC-side voltage causes the phase modules to underwork and the sub-modules to perform poorly. Moreover, when the compensation current output from the converter contains negative sequence components, the positive sequence three-phase voltage of the fundamental wave and the negative sequence compensation current causes a power shift. The specific analysis is as follows.

When the power system is unbalanced in three phases, the voltage of the grid contains negative sequence components, and the voltages of the three phases of the grid can be set as

$$\begin{cases} U_a = \sqrt{2}U_p \sin(\omega t) + \sqrt{2}U_n \sin(\omega t + \varphi) \\ U_b = \sqrt{2}U_p \sin\left(\omega t - 120^\circ\right) + \sqrt{2}U_n \sin\left(\omega t + \varphi + 120^\circ\right) \\ U_c = \sqrt{2}U_p \sin\left(\omega t + 120^\circ\right) + \sqrt{2}U_n \sin\left(\omega t + \varphi - 120^\circ\right) \end{cases} \tag{1}$$

In formula (1), U_p represents the effective value of the positive sequence voltage. U_n represents the effective value of the negative sequence voltage. φ represents the phase angle of the negative sequence voltage. The output current of the improved MMC-STATCOM converter in compensating the reactive power and negative sequence in the three-phase unbalanced condition is

$$\begin{cases} i_{ap} = \sqrt{2}I_p \cos(\omega t) + \sqrt{2}I_n \sin(\omega t + \phi) \\ i_{bp} = \sqrt{2}I_p \cos\left(\omega t - \frac{2}{3}\pi\right) + \sqrt{2}I_n \sin\left(\omega t + \frac{2}{3}\pi + \phi\right) \\ i_{cp} = \sqrt{2}I_p \cos\left(\omega t + \frac{2}{3}\pi\right) + \sqrt{2}I_n \sin\left(\omega t - \frac{2}{3}\pi + \phi\right) \end{cases} \tag{2}$$

In formula (2), I_p represents the effective value of the positive sequence current. I_n represents the effective value of the negative sequence current. ϕ represents the phase angle of the negative sequence current. The power absorbed by each phase of the grid is

$$\begin{cases} P_a = U_a \cdot i_{ap} \\ P_b = U_b \cdot i_{bp} \\ P_c = U_c \cdot i_{cp} \end{cases} \tag{3}$$

The power absorbed from the grid by each phase of the MMC-STATCOM converter rate from the grid are

$$\begin{cases} P_{ma} = P_a - i_{ap} L \dfrac{di_{ap}}{dt} \\ P_{mb} = P_b - i_{bp} L \dfrac{di_{bp}}{dt} \\ P_{mc} = P_c - i_{cp} L \dfrac{di_{cp}}{dt} \end{cases} \tag{4}$$

The average power absorbed by each phase of the converter in the fundamental cycle is

$$\begin{cases} \overline{P_{ma}} = U_p I_n \cos\phi + U_n I_n \cos(\varphi - \phi) \\ \qquad +U_n I_p cos\varphi \\ \overline{P_{mb}} = U_p I_n \cos\left(\phi - \frac{2}{3}\pi\right) + U_n I_n \cos(\varphi - \phi) \\ \qquad +U_n I_p cos\left(\varphi + \frac{2}{3}\pi\right) \\ \overline{P_{mb}} = U_p I_n \cos\left(\phi + \frac{2}{3}\pi\right) + U_n I_n \cos(\varphi - \phi) \\ \qquad +U_n I_p cos\left(\varphi - \frac{2}{3}\pi\right) \end{cases} \tag{5}$$

From formula (5), we can get

$$\overline{P_{ma}} + \overline{P_{mb}} + \overline{P_{mc}} = 3U_n I_n \cos(\varphi - \phi) \tag{6}$$

The deviation between the power absorption of each phase of the MMC-STATCOM converter and the power absorption of the three phases of the grid in the fundamental wave period is

$$\begin{cases} \overline{\Delta P_a} = U_p I_n \cos\phi + U_n I_p \cos\varphi \\ \overline{\Delta P_b} = U_p I_n \cos\left(\phi - \frac{2}{3}\pi\right) + U_n I_p \cos\left(\varphi + \frac{2}{3}\pi\right) \\ \overline{\Delta P_c} = U_p I_n \cos\left(\phi + \frac{2}{3}\pi\right) + U_n I_p \cos\left(\varphi - \frac{2}{3}\pi\right) \end{cases} \tag{7}$$

From the analysis of (5) and (6), we can conclude the following: the positive sequence voltage on the net side of the MMC-STATCOM converter and its output negative sequence compensation current, the interaction of the negative sequence voltage and positive sequence current on the net side leads to the transfer of active power between phases of the MMC-STATCOM converter, which also directly causes the unbalance of DC-side voltage between phases, but it does not cause the stability of DC-side voltage of the whole converter. Additionally, the negative sequence voltage on the net side and the negative sequence compensation current on the output of the MMC-STATCOM converter change the active power absorbed by the converter from the net side, which changes the DC-side voltage of the converter.

When the converter's phase-to-phase module loss is different, the negative sequence component can be injected in the current command value to change the converter's three phases to absorb power from the network side for controlling the phase-to-phase voltage of the converter. However, the negative sequence component method used also has relatively large drawbacks, because the negative sequence component of the compensating current output of the converter pollutes the grid environment by making additional negative sequence components in the grid. Therefore, this paper proposes an additional zero-sequence voltage in the phase-to-phase voltage balancing control to balance the DC-side voltage. The fundamental zero-sequence voltage and the positive-sequence current act to redistribute the power among the three phases of the converter.

Assume that the zero-sequence voltage injected into the converter is

$$U_0 = \sqrt{2}U \sin(\omega t + \theta) \tag{8}$$

In formula (8), U represents the effective value of the zero-sequence voltage, θ represents the zero-sequence phase angle, and the reference position is based on the grid phase A voltage. Combined with (2), the three-phase power change of the converter after zero sequence injection is:

$$\begin{cases} P_a^0 = UI_p \sin\theta - UI_p \cos\left(2\omega t + \frac{\pi}{2} + \theta\right) \\ +UI_n \cos(\phi - \theta) - UI_n \cos(2\omega t + \phi + \theta) \\ P_b^0 = UI_p \sin\left(\theta + \frac{2}{3}\pi\right) - UI_p \cos\left(2\omega t - \frac{\pi}{3} + \theta\right) \\ +UI_n \cos\left(\frac{2}{3}\pi + \phi - \theta\right) - UI_n \cos\left(2\omega t + \frac{2}{3}\pi + \phi + \theta\right) \\ P_c^0 = UI_p \sin\left(\theta - \frac{2}{3}\pi\right) - UI_p \cos\left(2\omega t + \frac{7\pi}{6} + \theta\right) \\ +UI_n \cos\left(\phi - \theta - \frac{2}{3}\pi\right) - UI_n \cos\left(2\omega t - \frac{2}{3}\pi + \phi + \theta\right) \end{cases} \tag{9}$$

The sum of all the equations in (9) is zero, which shows that the zero-sequence voltage injected into the converter does not affect the total power of the converter, and it only redistributes the power between phases. Therefore, in this paper, zero-sequence voltage is used in the phase-to-phase voltage balancing control to redistribute the phase-to-phase power and make the phase-to-phase DC-side voltage balanced. From (8), in a fundamental wave period, we get

$$\begin{cases} \overline{\Delta P_a^0} = UI_p \sin\theta + UI_n \cos(\phi - \theta) \\ \overline{\Delta P_b^0} = UI_p \sin\left(\theta + \frac{2}{3}\pi\right) + UI_n \cos\left(\phi - \theta + \frac{2}{3}\pi\right) \\ \overline{\Delta P_c{}^0} = UI_p \sin\left(\theta - \frac{2}{3}\pi\right) + UI_n \cos\left(\phi - \theta - \frac{2}{3}\pi\right) \end{cases} \tag{10}$$

The sum of equations in (10) is also zero, so the magnitude of the zero-sequence voltage U_0 can be obtained from (10):

$$\begin{aligned} U_0 = &\frac{y\overline{\Delta P_b^0} I_p + z\overline{\Delta P_a^0} I_p + y\overline{\Delta P_b^0} I_n \sin\phi}{(I_p + I_n)(I_n - I_p)} \sin(\omega t) \\ &+ \frac{z\overline{\Delta P_a^0} I_n \sin\phi - x\overline{\Delta P_a^0} I_n \cos\phi}{(I_p + I_n)(I_n - I_p)} \sin(\omega t) \\ &- \frac{y\overline{\Delta P_b^0} I_p \cos\phi + z\overline{\Delta P_a^0} I_n \cos\phi}{(I_p + I_n)(I_n - I_p)} \cos(\omega t) \\ &+ \frac{x\overline{\Delta P_a^0} I_n \sin\phi - x\overline{\Delta P_a^0} I_p}{(I_p + I_n)(I_p - I_n)} \cos(\omega t) \end{aligned} \tag{11}$$

The zero-sequence voltage command value injected into the converter is obtained from (11), where the positive current I_p and negative sequence current I_n, and the negative sequence current phase angle are obtained from the reactive power detection link of the load current. The phase ωt is derived from the grid phase lock loop. Fig.6 shows the block diagram of the converter phase-to-phase voltage control. First, the average value of the DC-side voltage of the converter's three phase modules is compared with the given value of the DC voltage, and then adjusted by the PI controller to obtain the power deviation to be adjusted for the phase module losses. The grid voltage is Pike transformed and inverse Pike transformed to obtain the positive sequence voltage U_p, negative sequence voltage U_n and negative sequence voltage phase angle φ.

Taking phase A as an example, the DC-side voltage variation is analyzed during the fundamental wave period as

$$\overline{\Delta U_a^0 i_{ap}} = \frac{C}{N} s \overline{\Delta U_{a\_ave}} \tag{12}$$

The zero-sequence voltage at the output of the MMC-STATCOM converter results in the power change absorbed in phase A versus the voltage change on the DC side as

$$\overline{\Delta P_a^0} = \frac{C}{N} s \overline{\Delta U_{a\_ave}} \tag{13}$$

By performing the Laplace transform on (13), we get

$$\frac{\Delta U_{a\_ave}(s)}{\Delta P_a^0(s)} = \frac{N}{Cs} \tag{14}$$

Using the PI controller, the block diagram of the parameter design of the phase-to-phase control system is shown in Fig. 7.

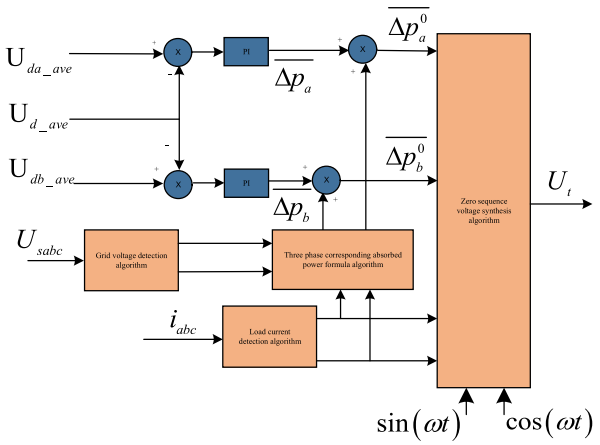

FIGURE 6. Phase-to-phase equalization control block diagram.

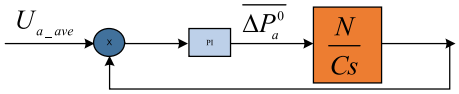

FIGURE 7. Block diagram of the design of the parameters of the PI controller of the phase-to-phase control sub-module.

E. IN-PHASE VOLTAGE CONTROL

The active current makes the total voltage on the DC side of the converter stable, and the zero-sequence voltage current is added to the converter command voltage to equalize the power between phases so that the intra-phase voltage is balanced. The intra-phase voltage needs to be balanced and controlled due to the different losses of each sub-module in the phase and the different charging and discharging of each sub-module. The intra-phase voltage balancing control block diagram is shown in Fig. 8. Taking phase A as an example to analyze the control process, the average value of phase A DC-side voltage is compared with the actual DC voltage of each sub-module and then adjusted by the PI controller to get the trim voltage command of phase A to the module. Then the trim voltage command is added to the original voltage command to get the final voltage command of the phase A module for MMC-STATCOM.

Each module fine-tunes the voltage command in the direction of the output current of the MMC-STATCOM converter, and the corresponding amount of its active power absorption is adjusted to control the voltage balance on the DC side of each module.

Generally, the response of the voltage loop is slow, and the expression for the DC-side voltage variation during the analysis of the fundamental cycle is

$$NC\frac{d\overline{\Delta U_{dc\_a1}}}{dt} = \Delta E_{a1} \tag{15}$$

In formula (15), ΔE_{a1} is the amount of regulation of each module in the AC side command voltage adjusted by the PI controller. The Laplace transform of formula (15) is further

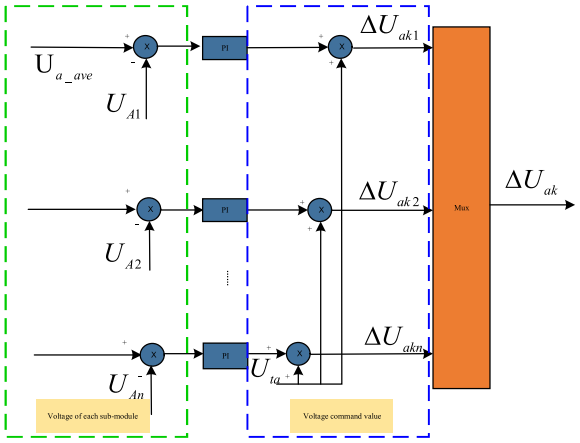

FIGURE 8. In-phase equalization control block diagram.

obtained as

$$\frac{\Delta U_{dc\_a1}(s)}{\Delta E_{a1}(s)} = \frac{1}{NC_s} \tag{16}$$

Using the PI controller, the controller parameters can be designed by (16), as shown in Fig.9.

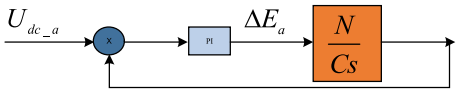

FIGURE 9. Block diagram of the design of the parameters of the PI controller of the in-phase control sub-module.

From the above three layers of control components, a complete control strategy for improved MMC-STATCOM in a grid environment is formed.

IV. MMC- STATCOM COMPENSATION UNDER THE SAME PHASE POWER SUPPLY

Negative sequence unbalance is an important manifestation of the problems in the traditional traction power supply system, but when the two-phase output of the balanced traction transformer in the substation meets the condition that the voltage and current are in phase, and when the effective values of the currents are equal, the negative sequence current can be eliminated, so the negative sequence component in the same phase power supply hardly affects the working compensation of MMC-STATCOM [28], [29], [30], [31].

The structure of the same phase traction power supply compensation system based on Vv transformer and MMC-STATCOM converter is shown in Fig.10. In Fig.10, the Vv-type main traction transformer changes the three-phase 110 kV voltage on the network side into single-phase voltage u_0, u_α, u_β, where u_α is the corresponding ac phase to supply the traction load and u_0, u_β is the corresponding ab and bc phases connected to the two sides of the MMC-STATCOM respectively.

Vv transformer secondary side output 2 amplitude of the same, phase difference of 60 degrees voltage U_α, U_β,

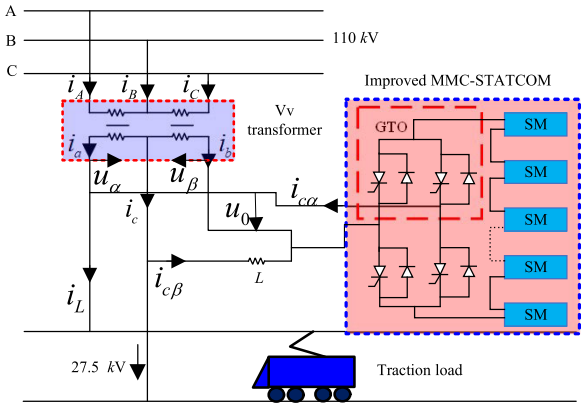

FIGURE 10. Topology of novel compensation system.

and the transformer secondary side a b port output current are I_a, I_b. When the output current of the corresponding phase on the secondary side of the transformer has the same amplitude and phase difference of 120 degrees, the three-phase current on the primary side of the transformer is completely symmetrical, and the secondary side output satisfies (17) through the compensation system, which can achieve the purpose of governing the negative sequence current.

$$\begin{cases} I_a = I_b \angle 120 \\ U_0 = U_\alpha \angle 60 = U_\beta \angle 120 \end{cases} \tag{17}$$

Setting the traction bus voltage rating to $U_T = 27.5$ kV, the transformer winding ab voltage u_0 can be obtained as follows:

$$u_0 = u_\beta = -\frac{27.5}{\sqrt{3}} kV \tag{18}$$

Let the load current be i_L, and the power factor be φ, and the relationship between the compensated ac port current I_a and the compensated current $I_{c\alpha}$ can be obtained as:

$$\begin{aligned} I_{c\alpha} &= \sqrt{{i_L}^2 + {I_a}^2 - 2 i_L I_a \cos(30 - \varphi)} \\ &= \sqrt{\frac{1}{3}\cos^2\varphi - \frac{\sqrt{3}}{3}\cos\varphi \sin\varphi + \sin^2\varphi} \end{aligned} \tag{19}$$

This gives the apparent power S_α on the α side as

$$S_\alpha = I_{c\alpha} U_\beta \tag{20}$$

Similarly, the expression of $I_{c\beta}$, can be obtained as

$$\begin{aligned} I_{c\beta} &= \sqrt{{i_L}^2 + {I_b}^2 - 2 i_L I_b \cos(90 - \varphi)} \\ &= \sqrt{\frac{1}{3}\cos^2\varphi - \frac{\sqrt{3}}{3}\cos\varphi \sin\varphi + \sin^2\varphi} \end{aligned} \tag{21}$$

From the above analysis, the application and compensation relations of the improved MMC-STATCOM converter in the traction power supply system are obtained.

V. SIMULATION EXPERIMENTS

To verify the effectiveness and correctness of the improved MMC-STATCOM converter topology compensation capability and DC voltage three-level control strategy, the new converter is modeled in the traction power supply environment for simulation experiments.

The MMC- STATCOM simulation model is built in the MATLAB/Simulink simulation platform, and the simulation parameters are shown in Table 2.

TABLE 2. Simulation parameters.

Parameter name	Parameter value
Power voltage/kV	110
Transformer ratio	110/27.5
Grid frequency /Hz	50
Number of submodules	9
AC side connection inductance /mH	5
DC side capacitance /mF	15
DC link voltage reference value /kV	50

A. CONTROL SIMULATION OF MMC-STATCOM STRUCTURE

In the grid environment, the MMC- STATCOM simulation model is built in MATLAB/Simulink simulation platform, and the initial load active power is 25 MW and reactive power is 5 Mvar. At 0.1 s, the MMC-STATCOM converter starts to work to verify the compensation effect.

The waveform curves of zero-sequence voltage and phase-to-phase capacitance voltage are shown in Fig.11 and Fig.12, respectively. Fig.11 shows that the zero-sequence voltage is injected into the MMC-STATCOM at 0.1 s, which balances the DC-side capacitance voltage. The balancing control method in this paper injects zero-sequence voltage to achieve phase power redistribution and phase voltage balancing, and the phase-to-phase capacitance voltage waveform curves in Fig.12 show the effectiveness and correctness of this control method.

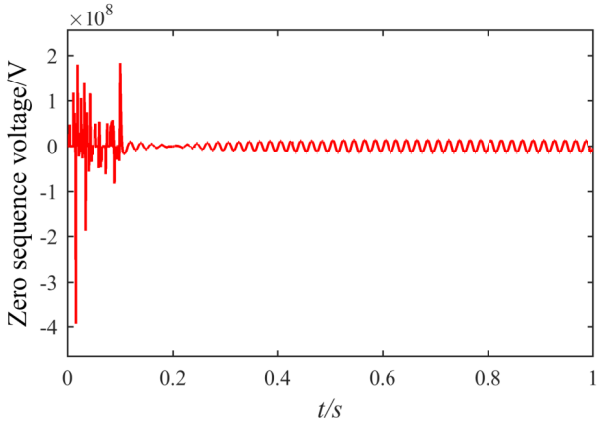

FIGURE 11. Zero sequence voltage.

Fig.13 shows the MMC-STATCOM output B-phase grid voltage and the B-phase MMC-STATCOM output compensation current waveform, the B-phase grid voltage waveform

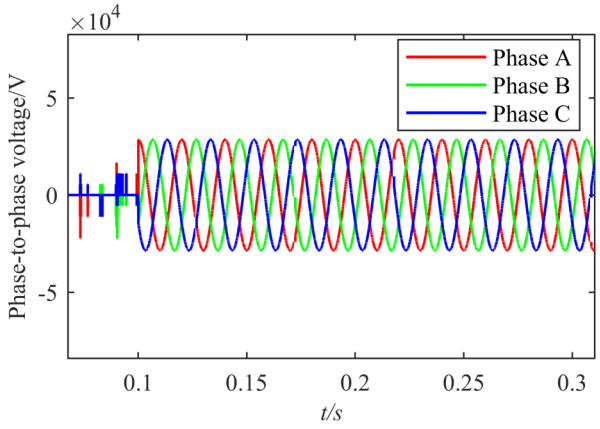

FIGURE 12. Phase-to-phase capacitor voltage.

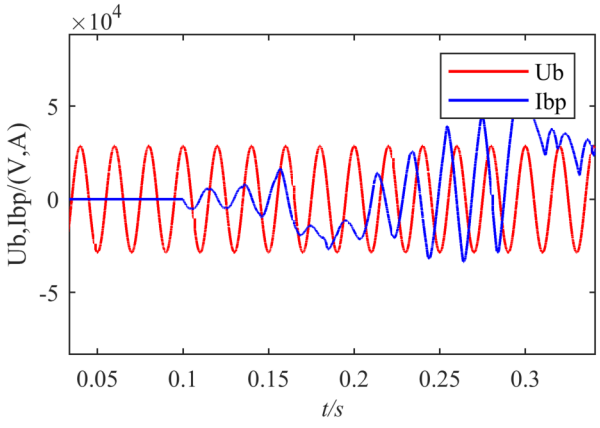

FIGURE 13. B-phase grid voltage and B-phase MMC-STATCOM output compensation current.

is a relatively good sine wave, and the B-phase compensation current waveform of the MMC-STATCOM output from 0.1 s shows also output compensation current with the load change. Fig.14 shows the MMC-STATCOM output B-phase DC-side voltage and B-phase upper and lower two module voltage waveforms, it can be seen that the B-phase DC-side voltage is stable around 50 kV, which indicates that the total DC-side control strategy is correct and effective, and the upper and lower two module output voltage fluctuation range is between 0-6 kV, which also indicates the output voltage of the upper and lower modules fluctuates between 0-6 kV, which also shows the effectiveness of the three-level control strategy adopted in this paper.

Fig.15 shows the waveforms of the MMC-STATCOM dynamically compensating the B-phase current, B-phase grid voltage and B-phase DC measurement voltage when the command current is flipped from 10 A to -10 A, which shows that the MMC-STATCOM can accurately and quickly compensate dynamically, and the DC measurement voltage is also stable. Fig.16 shows the B-phase negative sequence compensation current output by MMC-STATCOM when the load is unbalanced and sudden change, and the three-phase DC measured voltage fluctuates between 0-6 kV. It can be

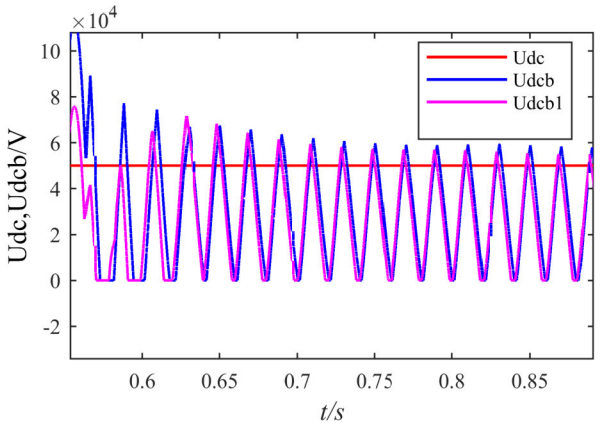

FIGURE 14. B-phase DC side voltage and B-phase H-bridge upper and lower module voltage waveforms.

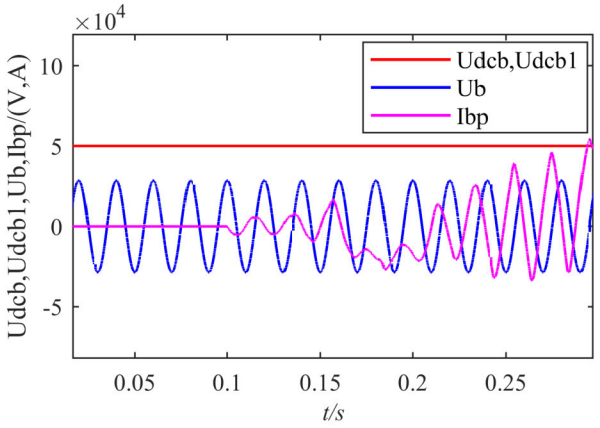

FIGURE 15. B-phase grid voltage, DC side voltage and compensation current output by B-phase MMC-STATCOM.

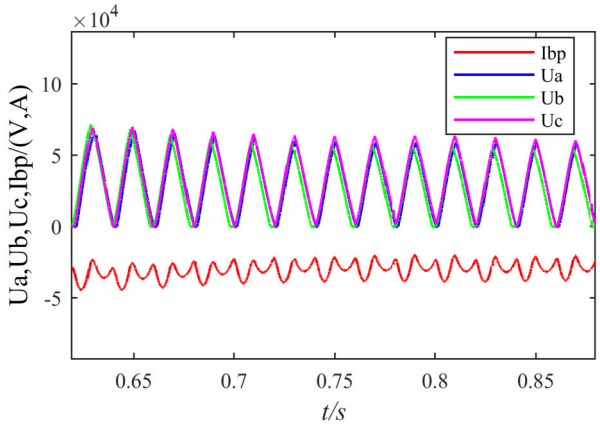

FIGURE 16. B-phase compensation current and three-phase DC side voltage waveform output by MMC-STATCOM when the load is unbalanced.

seen that MMC-STATCOM can compensate the unbalanced load and control the stability of DC-side voltage when the load is unbalanced, which also further illustrates the effectiveness of the three-level control method adopted in this paper for the DC-side of the converter, which is the

guarantee of stable compensation and normal operation of MMC-STATCOM converter.

B. COMPENSATION FOR SAME-PHASE TRACTION POWER SUPPLY

To verify the correctness and effectiveness of the MMC-STATCOM converter and Vv wired intra-phase traction power supply scheme in this paper, a simulation model of the system based on MATLAB/Simulink is built.

To reflect the fluctuation of traction load and the good dynamic compensation ability of the MMC-STATCOM converter, it is assumed that the initial traction load is 10 MVA and the power factor is 0.85. The MMC-STATCOM starts to work at 0.2 s, at which time the power quality compensation target is set to full compensation.

The simulation results are shown in Fig.17-Fig.22. Fig.17 shows the traction load current, the load current waveform is a smooth curve with good power quality. Fig.18 shows the network side voltage waveform after compensation, the voltage is a three-phase symmetric waveform curve with the amplitude of 110 kV. Fig.19 shows the network side current waveform after compensation, in the time period of 0-0.2 s, the MMC-STATCOM converter is not put into operation. In the time period of 0-0.2 s, the MMC-STATCOM converter is not put into operation, and after 0.2 s MMC-STATCOM compensation, the three-phase current waveform on the network side indicates good current power quality.

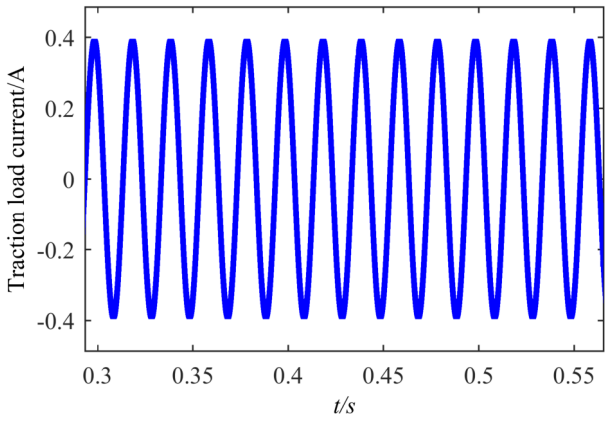

FIGURE 17. Load current waveform.

Fig.20 shows the secondary output of Vv transformer with two voltages of 40 V amplitude and 120 degrees phase difference, and the primary three phase currents of the transformer are perfectly symmetrical, which shows that the secondary output satisfies the equation (17) through the compensation system to achieve the purpose of controlling the negative sequence current. Fig.21 shows the MMC-STATCOMM converter port compensation current, and Fig.22 shows the MMC-STATCOMM converter port compensation current, after 0.2 s MMC-STATCOM converter input, MMC-STATCOM provides the compensation current with the amplitude of 35 A. The distribution of compensation

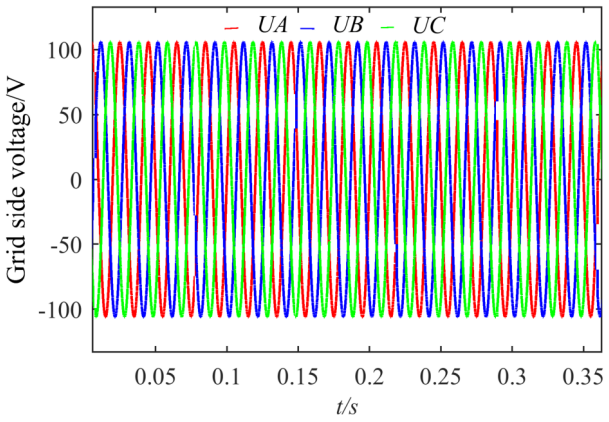

FIGURE 18. Grid side voltage waveform after compensation.

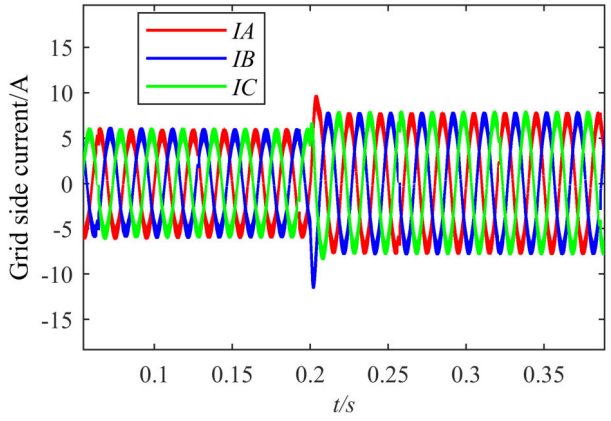

FIGURE 19. Grid side current waveform after compensation.

current waveform curve shows that MMC-STATCOM has good dynamic The distribution of the compensation current waveform shows that the MMC-STATCOM has good dynamic tracking compensation characteristics.

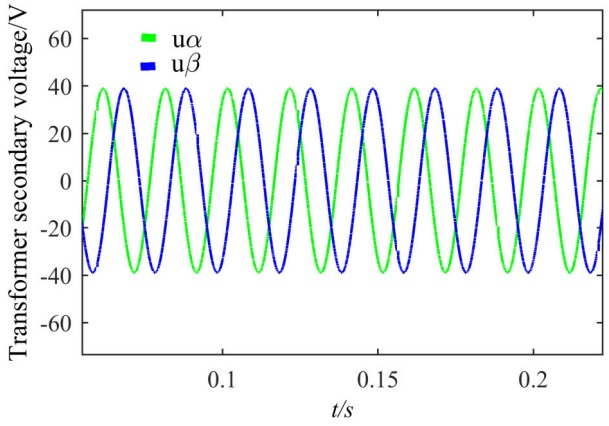

FIGURE 20. Transformer secondary side voltage.

C. ANALYSIS OF POWER SUPPLY COMPENSATION SCHEME

After the theoretical analysis and simulation verification of the above paper, the compensation schemes are analyzed and compared, and the results are shown in Table 3.

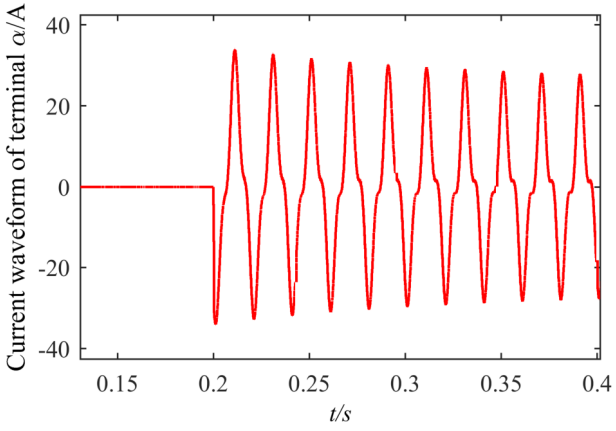

FIGURE 21. MMC-STATCOM α terminal current.

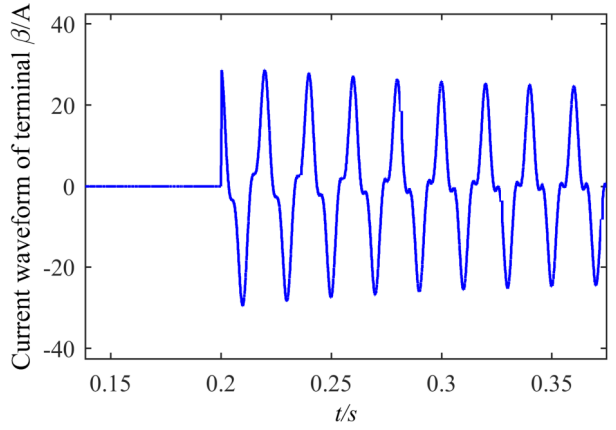

FIGURE 22. MMC-STATCOM β terminal current.

TABLE 3. Comparison of compensation schemes.

Type	traditional MMC	Cascade STATCOM	MMC-STATCOM
Level	2K+1	2K+1	2K+1
Switches	4K	4K	2K+4
Three-phase unbalance degree/%	0.7	0.98	0.96
Output power of converters/(MVA)	4.57	1.65	1.38
Total harmonic distortion rate	1.08	1.27	1.03

As can be seen from Table 3, the improved MMC-STATCOM scheme in this paper can reduce the number of power switching devices when the number of levels is 2K+1, so the scheme is more cost-effective. When the processing effect of each compensation scheme is similar, the output powers of the converter on both sides of MMC-STATCOM in the new compensation system are clearly much lower than those in the conventional compensation system. When the traction side is under heavy load, the three compensation systems are compared, and the output powers of both sides of the MMC-STATCOM converter are the largest. In terms of total harmonic distortion rate, the improved MMC-STATCOM has a lower total harmonic distortion rate. This verifies the above derivation that the minimum compensation capacity of active devices in the new compensation system is lower than that in the conventional compensation system, and the homogeneous power supply scheme of the new compensation system in this paper can also reduce the procurement cost.

VI. CONCLUSION

By studying and analyzing the cascaded MMC converter topology, this paper proposes an improved MMC-STATCOM converter topology. Compared with the cascaded MMC converter topology, the improved MMC-STATCOM converter topology can greatly reduce the number of power switching elements cascaded at low voltage. Moreover, this paper conducts an in-depth study on the improved MMC-STATCOM converter's DC-side voltage control to build a three-level control system including DC-side total voltage control, phase-to-phase voltage balancing control, and intra-phase voltage balancing control. The DC-side total voltage control of the improved MMC-STATCOM topology is the size of active power obtained from the power system by the three-phase MMC-STATCOM converter, and the obtained active power contains only the fundamental wave positive sequence component to ensure the power quality of the power system. Phase-to-phase voltage balancing control is the second layer of control, which adds zero-sequence voltage to the converter so that the power between the three phases of the converter can be balanced to achieve the purpose of rapid regulation of real-time changes in the phase voltage; in addition, no additional negative sequence components flow into the power system. Intra-phase voltage balancing control is the third level of control, which provides voltage control of each phase sub-module of the converter to ensure that the three-phase DC-side voltage of the converter is equal to the given value. Finally, a simulation model is built to verify the compensation feasibility of the converter structure in both grid and traction power supply environments. The results prove the rationality and effectiveness of the proposed DC-side total voltage control method and have certain reference significance in engineering applications.

AUTHOR CONTRIBUTIONS

Yong Zhou: conceptualization, formal analysis, methodology, software, writing-original draft, and validation; Minan Tang: conceptualization, funding acquisition, investigation, project administration, supervision, writing-review and editing, and formal analysis; and Weili Liu: conceptualization, formal analysis, software, and investigation.

DECLARATIONS

This manuscript has not been published or presented elsewhere in part or in its entirety and is not under consideration by any other journal. We have read and understood your journal's policies, and we believe that neither the manuscript nor the study violates any of these. There are no conflicts of interest to declare.

REFERENCES

[1] G. Q. Li, Y. Yang, and Y. C. Xin, "An improved hybrid half-bridge MMC with fault blocking capability," *Electr. Power Autom. Equip.*, vol. 41, pp. 166–173, Dec. 2021.

[2] Q. T. Wang, G. Wang, and Q. Wu, "Topological analysis of a capacitor clamp sub-module with fault handling capability," *Chin. J. Railway Sci. Eng.*, vol. 16, pp. 1560–1568, Jun. 2019.

[3] G. Wei, "In-phase traction power supply system based on V-connection," *Electr. Power Autom. Equip.*, vol. 30, pp. 60–65, Dec. 2010.

[4] C. P. Wu, A. Luo, and X. Y. Xu, "Negative sequence and harmonic compensation method for high-speed railway traction power supply system using V/V transformer," *Chin. J. Electr. Eng.*, vol. 30, pp. 111–117, Jun. 2010.

[5] G. Wei, "Research on in-phase traction power supply system based on MMC and Vv wiring," *Chin. J. Railway Sci. Eng.*, vol. 16, pp. 2077–2082, Aug. 2019.

[6] D. Pan, M. S. Zhang, and H. Y. Zhang, "Research on DC side voltage control strategy of D-STATCOM based on MMC," *Power Electron. Technol.*, vol. 55, pp. 115–119, Sep. 2021.

[7] X. He, J. Peng, and P. Han, "A novel advanced traction power supply system based on modular multilevel converter," *IEEE Access*, vol. 7, pp. 165018–165028, 2019.

[8] M. Lei, Y. Wang, and C. Zhao, "Optimized operation of the full-bridge five-branch modular multilevel converter for power quality enhancement of cophase railway power system," *IEEE Trans. Transport. Electrific.*, vol. 8, no. 1, pp. 590–604, Mar. 2022.

[9] M. Lei, C. Zhao, Z. Li, and J. He, "Circuit dynamics analysis and control of the full-bridge five-branch modular multilevel converter for comprehensive power quality management of cophase railway power system," *IEEE Trans. Ind. Electron.*, vol. 69, no. 4, pp. 3278–3291, Apr. 2022.

[10] X. F. Yang and Q. L. Zheng, "General circulation suppression strategy based on MMC circulation model," *Chin. J. Electr. Eng.*, vol. 32, pp. 59–65, Dec. 2012.

[11] Y. K. Xia, F. L. Zhou, and M. U. Chen, "Hybrid compensation in-phase power supply scheme for high-speed railway V-type wiring traction transformer," *J. Electr. Power Syst. Autom.*, vol. 29, pp. 89–94, Jul. 2017.

[12] H. Akagi, "Classification, terminology, and application of the modular multilevel cascade converter (MMCC)," *IEEE Trans. Power Electron.*, vol. 26, no. 11, pp. 3119–3130, Nov. 2011.

[13] S. Vazquez, J. I. Leon, and J. M. Carrasco, "Analysis of the power balance in the cells of a multilevel cascaded H-bridge converter," *IEEE Trans. Power Electron.*, vol. 57, no. 7, pp. 2287–2296, Jul. 2010.

[14] J. A. Barrena, L. Marroyo, M. Á. Rodriguez Vidal, and J. R. T. Apraiz, "Individual voltage balancing strategy for PWM cascaded H-bridge converter-based STATCOM," *IEEE Trans. Ind. Electron.*, vol. 55, no. 1, pp. 21–29, Jan. 2008.

[15] S.-F. Chou, B.-S. Wang, S.-W. Chen, C.-T. Lee, P.-T. Cheng, H. Akagi, and P. Barbosa, "Average power balancing control of a STATCOM based on the cascaded H-bridge PWM converter with star configuration," in *Proc. IEEE Energy Convers. Congr. Expo.*, Sep. 2013, pp. 3893–3901.

[16] L. L. Zhu and J. Chen, "Static reactive power generator based on improved MMC," *Southern Power Grid Technol.*, vol. 15, pp. 47–53, Jul. 2021.

[17] X. Liu, Z. A. Tang, and K. Zhang, "Three-level balance control of MMC-STATCOM capacitor voltage based on energy analysis," *High Voltage Technol.*, vol. 44, pp. 2222–2230, Jul. 2018.

[18] G. X. Qiu, P. Y. Peng, and C. Wang, "Research on the compensation strategy of MMC-STATCOM under the condition of unbalanced load," *Electr. Power Eng. Technol.*, vol. 39, pp. 35–42, Mar. 2020.

[19] J. Yu, Z. Zhang, and Z. Xu, "An equivalent calculation method for pole-to-ground fault transient characteristics of symmetrical monopolar MMC based DC grid," *IEEE Access*, vol. 8, pp. 123952–123965, 2020.

[20] K. Dai, C. Yu, and Y. F. Ding, "Modeling and hierarchical control of improved MMC-STATCOM," *J. Electrotech. Technol.*, vol. 28, pp. 44–51, Dec. 2013.

[21] Y. Xu, Z. Xu, Z. Zhang, and H. Xiao, "A novel circulating current controller for MMC capacitor voltage fluctuation suppression," *IEEE Access*, vol. 7, pp. 120141–120151, 2019.

[22] Y. Neyshabouri, S. K. Chaudhary, R. Teodorescu, R. Sajadi, and H. Iman-Eini, "Improving the reactive current compensation capability of cascaded H-Bridge based STATCOM under unbalanced grid voltage," *IEEE J. Emerg. Sel. Topics Power Electron.*, vol. 8, no. 2, pp. 1466–1476, Jun. 2020.

[23] L. d. N. Gomes, A. J. G. Abrantes-Ferreira, and L. G. B. Rolim, "Synchronverter-based STATCOM with voltage imbalance compensation functionality," *IEEE Trans. Ind. Electron.*, vol. 69, no. 5, pp. 4836–4844, May 2022.

[24] T. M. Chen, G. H. Zeng, and J. Wang, "Phase-shift modulation strategy of modular multi-level DC converter to suppress current ripple," *Autom. Electr. Power Syst.*, vol. 45, pp. 206–214, Jul. 2021.

[25] S. Ali, Z. Ling, K. Tian, and Z. Huang, "Recent advancements in submodule topologies and applications of MMC," *IEEE J. Emerg. Sel. Topics Power Electron.*, vol. 9, no. 3, pp. 3407–3435, Jun. 2021.

[26] L. L. Hi, Z. K. Shuai, and J. J. Shan, "Comparative analysis of multi-carrier modulation strategies of MMC," *J. Power Supply*, vol. 17, pp. 56–64, Dec. 2019.

[27] M. Tang, Y. Zhou, K. Liang, X. Liu, and X. Tong, "Cophase traction power supply system based-MMC-Vv wiring," *IEEE Access*, vol. 10, pp. 96016–96025, 2022.

[28] L. Z. Yi, L. Liu, and X. H. Huang, "Comparison and analysis of optimal modulation strategies for output current harmonics of modular multilevel converters," *J. Electr. Power Syst. Autom.*, vol. 32, pp. 85–94, May 2020.

[29] G. P. Cui, L. F. Luo, and Y. Li, "Electrified railway co-phase power supply system based on new YNvd balance transformer," *Power Autom. Equip.*, vol. 39, pp. 158–163, Feb. 2019.

[30] J. X. Zhou, L. L. Luo, and H. L. Wang, "In-phase power supply system based on double-star multilevel power flow controller and YNvd transformer," *Power Syst. Protection Control*, vol. 47, pp. 9–16, Apr. 2019.

[31] Q. Z. Li, S. F. Xie, and L. Y. Zhang, "Negative sequence compensation model and control strategy for electrified railway using YNd-SVG," *High Voltage Technol.*, vol. 47, pp. 1740–1752, May 2021.

YONG ZHOU received the bachelor's degree in power engineering and management from Lanzhou Jiaotong University, China, in 2016, where he is currently pursuing the master's degree in electronic information. His research interests include the power supply quality control of power systems and traction power supply compensation.

MINAN TANG (Senior Member, IEEE) received the Ph.D. degree in transportation information engineering and control from Lanzhou Jiaotong University, China, in 2011. He was a Postdoctoral Researcher in intelligent traffic control with the Lanzhou University of Technology, China, in 2012. He is currently a Professor and a Doctoral Supervisor with the College of Automation and Electrical Engineering, Lanzhou Jiaotong University. His research interests include complex intelligent control systems, intelligent transportation systems, process control systems, and the power supply quality control of power systems.

WEILI LIU received the bachelor's degree in rail transit signal and control from the Henan University of Technology, China, in 2019, and the master's degree in control engineering from Lanzhou Jiaotong University, China, in 2022. Her research interests include power quality governance, image processing, and traction power supply for power systems.